JACS
JOURNAL OF THE AMERICAN CHEMICAL SOCIETY
Communication
pubs.acs.org/JACS

Doping-Induced Anisotropic Self-Assembly of Silver Icosahedra in $[Pt_2Ag_{23}Cl_7(PPh_3)_{10}]$ Nanoclusters

Megalamane S. Bootharaju,[†] Sergey M. Kozlov,[†] Zhen Cao,[†] Moussab Harb,[†] Niladri Maity,[†] Aleksander Shkurenko,[‡] Manas R. Parida,[§] Mohamed N. Hedhili,[∥] Mohamed Eddaoudi,[‡] Omar F. Mohammed,[§] Osman M. Bakr,*[,§] Luigi Cavallo,*[,†] and Jean-Marie Basset*[,†]

[†]KAUST Catalysis Center, [‡]Functional Materials Design, Discovery and Development Research Group (FMD3), Advanced Membranes and Porous Materials Center, [§]KAUST Solar Center, and [∥]Imaging and Characterization Laboratory, King Abdullah University of Science and Technology (KAUST), Thuwal 23955-6900, Saudi Arabia

Supporting Information

ABSTRACT: Atomically precise self-assembled architectures of noble metals with unique surface structures are necessary for prospective applications. However, the synthesis of such structures based on silver is challenging because of their instability. In this work, by developing a selective and controlled doping strategy, we synthesized and characterized a rod-shaped, charge-neutral, diplatinum-doped Ag nanocluster (NC) of $[Pt_2Ag_{23}Cl_7(PPh_3)_{10}]$. Its crystal structure revealed the self-assembly of two Pt-centered Ag icosahedra through vertex sharing. Five bridging and two terminal chlorides and 10 PPh_3 ligands were found to stabilize the cluster. Electronic structure simulations corroborated structural and optical characterization of the cluster and provided insights into the effect of the Pt dopants on the optical properties and stability of the cluster. Our study will open new avenues for designing novel self-assembled NCs using different elemental dopants.

Precise control over the composition, size, shape, and monodispersity of nanoparticles (NPs) is one of the biggest challenges in materials science. Polydispersity, a wide distribution of size and shape of NPs, prevents the achievement of precisely defined functional properties and hinders direct comparison and evaluation of NPs.[1] However, advanced synthetic routes, involving protecting ligands, allow control of the size and composition of NPs from a few tens to hundreds of metal atoms. These methods led to the development of a distinct class of materials called atomically precise NPs, nanoclusters (NCs), or nanomolecules.[2−13] NCs gained an extensive research interest both in fundamental and applied sciences not only because of their intriguing optical,[14,15] photophysical,[16,17] and chemical properties[5,18] (originating from ultrasmall size and discrete energy levels) but also for their potential applications in sensing,[5] catalysis,[19,20] bioimaging,[3] and energy conversion.[5]

Most of the current research has focused mainly on Au NCs[2,21] (e.g., Au_{18}, Au_{25}, Au_{38}, Au_{102}, and Au_{133}) because of their high stability, while the properties of the analogous Ag NCs have largely been unexplored. Nevertheless, a handful of Ag NCs such as Ag_{21},[22] Ag_{25},[14] Ag_{29},[16] Ag_{44},[23,24] Ag_{67},[25] Ag_{136},[26] and Ag_{374},[26] including their X-ray crystal structures, have been reported. Subsequently, AgAu and other alloy NCs[27,28] have also been synthesized to obtain enhanced optical[29−31] and catalytic[19] properties.

The majority of metal NCs reported are isotropic and approximately spherical. Although a few anisotropic Au NCs have been developed,[2] those of Ag[25] are rare. In addition to anisotropy and metal nuclearity, NCs containing self-assembled metal nanobuilding blocks[32] are highly desired for applications, as they would provide distinct surface structures. The use of labile ligands (e.g., phosphines) and nonbulky ligands (e.g., halides) for these self-assembled nanostructures would make their surface more accessible. Such self-assembly of metal nanobuilding blocks was previously observed in Au[7,32] and its heteroatom-doped NCs,[33−39] such as $[MAu_{12}Ag_{12}(PPh_3)_{10}Cl_7]^+$ (M = Pt, Ni; PPh_3 = triphenylphosphine) and $[Pt_2Au_{10}Ag_{13}(PPh_3)_{10}X_7]$ (X = Cl, Br), as a result of their high stability provided by more-noble Au atoms. However, the synthesis of these NCs involves multiple steps and preprepared complexes as metal precursors. Moreover, analogous pure Ag or Ag-based doped NCs have not been achieved to date because of synthetic challenges and instability issues caused by the oxidation of less-noble Ag atoms.

In this work, we designed a single-step reaction to synthesize a heteroatom-doped Ag NC comprising self-assembled Ag building blocks by using Pt as the dopant and a labile phosphine (PPh_3) and simple Cl^- as ligands. Pt was chosen as the dopant since Ag and Pt have different atomic radii (1.65 and 1.77 Å, respectively), which was envisaged to prevent the formation of NCs with various degrees of doping. Our synthetic protocol involves the $NaBH_4$ reduction of a mixture of readily available Ag and Pt precursors, $AgNO_3$ and $Na_2PtCl_6{\cdot}6H_2O$, in the presence of PPh_3 in CH_3OH and CH_2Cl_2 as cosolvents (see the Supporting Information (SI) for details). The final NC in CH_2Cl_2 was crystallized by layering with hexane. Single-crystal X-ray diffraction (SCXRD) and high-resolution electrospray ionization mass spectrometry (ESI-MS) unambiguously revealed the composition of the synthesized product to be $[Pt_2Ag_{23}Cl_7(PPh_3)_{10}]$, possessing self-assembled Ag icosahedra (vide infra).

Received: November 17, 2016
Published: January 9, 2017

DOI: 10.1021/jacs.6b11875
J. Am. Chem. Soc. 2017, 139, 1053−1056

As we had in mind, the introduction of Pt as a dopant was crucial to obtain a self-assembled cluster with a precise molecular formula and structure. In the absence of the Pt source, the synthesized product (Figure S1) was a hydride-rich $[Ag_{18}H_{16}(PPh_3)_{10}]^{2+}$ cluster rather than $[Ag_{25}Cl_7(PPh_3)_{10}]^q$ (q = charge). However, this Ag_{18} NC was unstable in common solvents, such as CH_2Cl_2, preventing the formation of single crystals for XRD. Therefore, introducing Pt ions not only enhanced the stability of the final product $[Pt_2Ag_{23}Cl_7(PPh_3)_{10}]$ in CH_2Cl_2 but also facilitated the growth of single crystals.

SCXRD analysis of the $[Pt_2Ag_{23}Cl_7(PPh_3)_{10}]$ crystals revealed that it crystallizes in space group $P2_1/m$ (Table S1), and the unit cell contains two clusters (Figure S2). This cluster was found to be charge-neutral, as no counterions were found in its crystal structure, consistent with the ESI-MS and theoretical results (vide infra). Moreover, the density functional theory (DFT)-optimized geometry of $[Pt_2Ag_{23}Cl_7(PPh_3)_{10}]$ is very similar to the X-ray structure. The root-mean-square deviation between the two structures is 0.13 Å when counted on all atoms excluding C and H (0.26 Å when only H is excluded). The total structure of the cluster comprising a Pt_2Ag_{23} metal rod is shown in Figure 1.

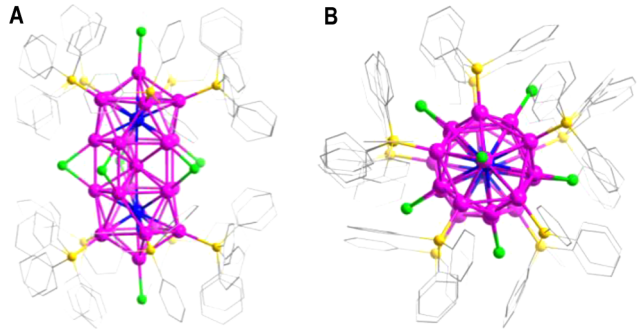

Figure 1. (A) Side view and (B) top view of the $[Pt_2Ag_{23}Cl_7(PPh_3)_{10}]$ cluster. Color legends: cyan, Ag; blue, Pt; yellow, P; green, Cl; gray, C. The H atoms of the ligands have been omitted for clarity.

Detailed structure analysis of the cluster revealed the presence of two $PtAg_{12}$ icosahedra with the Pt at the center (Figure 2A) that are self-assembled through vertex sharing to form the Pt_2Ag_{23} metal structure in a rod shape (Figures 1A and 2B). The length of the rod is 1.106(1) nm (the distance between the two terminal or apex Ag atoms). The average Ag−Ag and Ag−Pt bond distances in the $PtAg_{12}$ icosahedra are 2.88 Å (as in bulk Ag[16]) and 2.74 Å, respectively, indicating strong interactions among the Ag atoms. However, the average distance between the Ag atoms that connect the two icosahedra is 2.94 Å. The Pt_2Ag_{23} appeared to have an imperfect rod shape, as it is slightly bent (since the angle between the lines from the central vertex-shared Ag atom to the apex Ag atoms deviates by 3.4° from 180°). This bending would have resulted in clearly different Ag−Ag bonds between the two icosahedra from those within an icosahedron.

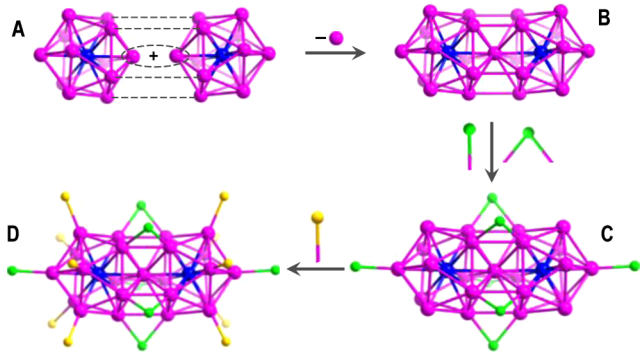

Figure 2. (A) Vertex Ag atoms of two $PtAg_{12}$ icosahedra being shared and connected are shown with a dotted ellipse and dotted lines, respectively. (B) Biicosahedral Pt_2Ag_{23} rod. (C) Bridging and terminal chlorides bind with the structure shown in (B) to form $Pt_2Ag_{23}Cl_7$. (D) Capping with the 10 P atoms of 10 PPh_3 ligands gives $Pt_2Ag_{23}Cl_5P_{10}$. Color legends are the same as in Figure 1.

Seven Cl^- ligands were found to protect the Pt_2Ag_{23} framework in two different binding modes. Five Cl^- ions act as bridging ligands, connecting the two $PtAg_{12}$ icosahedra to form the structure shown in Figure 2C. The remaining two Cl^- ions are connected to the two terminal Ag atoms of the Pt_2Ag_{23} rod in the form of dangling Ag−Cl bonds. The average Ag−Cl bond length is ∼2.50 Å. The P atoms of the 10 PPh_3 ligands bind with the remaining 10 uncoordinated Ag sites to give the total $[Pt_2Ag_{23}Cl_7(PPh_3)_{10}]$ structure (Figure 2D). The average Ag−P distance was found to be 2.42 Å. The top view of the cluster (Figure 1B) shows that the PPh_3 ligands in the two icosahedra are in an eclipsed configuration. Alternatively, the Pt_2Ag_{23} structure of the cluster can be interpreted on the basis of the connectivity of the ligands and metal atoms. A linear Pt−Ag−Pt metal core is located deep inside the cluster and not connected to ligands. The remaining 22 Ag atoms form a closed rod-like morphology. Encapsulation of the Pt_2Ag bimetallic core within the Ag_{22} shell or rod produces the total structure of the Pt_2Ag_{23} framework (Figure S3).

Subsequently, ESI-MS of the cluster was performed to support the formula and the charge obtained from SCXRD. The absence of mass signals for the cluster in either positive or negative ion mode confirmed the neutral charge state. However, a mass peak at $m/z \approx 3004$ with a charge of 2+ was observed for a cluster solution that was mixed with Cs_2CO_3 solution (Figure S4A,B). The total mass of this peak corresponds to $[Pt_2Ag_{23}Cl_7(PPh_3)_{10}]Cs_2$, and it was further verified by a perfect match of the experimental mass spectrum with the corresponding simulated one (Figure S4C). The existence of the cluster in solution was confirmed from a large shift and broadening of the ^{31}P NMR peak (2.83 ppm) along with a slight shift of the ^1H NMR peaks (∼7.32 ppm) of the cluster from those of free PPh_3 (−5.42 and ∼7.23 ppm, respectively) (Figures S5 and S6). Further broadening and shifting of the ^{31}P NMR peaks at low temperature (Figure S7) indicated partial restricted rotations of the PPh_3 ligands bound to cluster. X-ray photoelectron spectroscopy (XPS) shows the presence of all of the expected elements in the cluster (Figure S8). The Ag $3d_{5/2}$ peak at 367.8 eV suggests the Ag valence state to be between Ag(0) and Ag(I). The majority of the Pt was present as Pt(0), consistent with the SCXRD results. A minor fraction of unreacted Pt(II) species, which could not be removed by solvent washing, was also identified. The yield of the cluster was ∼24% (based on Ag atoms). The cluster is sensitive to light in both the solid and solution states. Nevertheless, it is stable in the dark for a day in CH_2Cl_2 and more than 25 days in the solid state (Figure S9).

The optical properties and electronic structure of $[Pt_2Ag_{23}Cl_7(PPh_3)_{10}]$ were further studied both experimentally and theoretically using summation over empty states DFT (SOS-DFT) and time-dependent DFT (TD-DFT). The

DOI: 10.1021/jacs.6b11875
J. Am. Chem. Soc. 2017, 139, 1053−1056

experimental absorption spectrum of $[Pt_2Ag_{23}Cl_7(PPh_3)_{10}]$ shows well-defined multiple features at 338, 364, 442, 487, and 562 nm (Figure 3). Its optical gap of ~1.5 eV (Figure 3

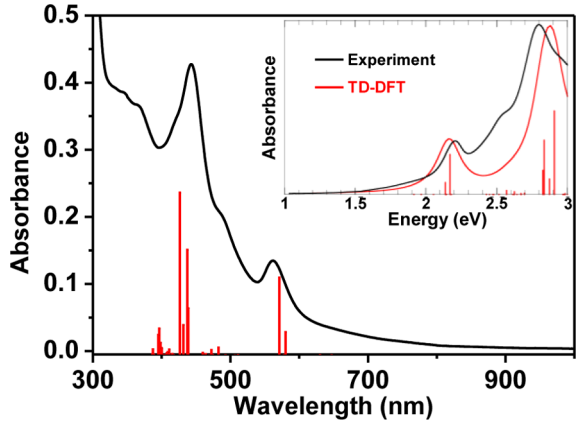

Figure 3. Experimental UV−vis spectrum of $[Pt_2Ag_{23}Cl_7(PPh_3)_{10}]$ (black) compared with the excitation energies and oscillator strengths calculated by TD-DFT for $[Pt_2Ag_{23}Cl_7(P(CH_3)_3)_{10}]$ (red). Inset: corresponding UV−vis data on the energy scale; the red curve was constructed via Lorentzian broadening of 0.1 eV.

inset) is close to the calculated DFT HOMO−LUMO gap of 1.62 eV for the neutral cluster. The experimental optical spectrum is in good agreement with the TD-DFT results calculated for the cluster with simplified ligands, $[Pt_2Ag_{23}Cl_7(P(CH_3)_3)_{10}]$. Such simplification of the ligands was shown by SOS-DFT not to affect the peak positions (Figure S10). The main TD-DFT calculated excitations of $[Pt_2Ag_{23}Cl_7(P(CH_3)_3)_{10}]$ are at ~430 and 571 nm, corresponding to the dominant experimental features at 442 and 562 nm (Figure 3). Much less intense calculated peaks at 482 nm correspond to the experimental shoulder at 487 nm. It should be noted that according to the calculations, $[Pt_2Ag_{23}Cl_7(PPh_3)_{10}]$ clusters with charges of +1 or +2 have HOMO−LUMO gaps of ~0.5 eV and optical spectra very different from the experimental ones (Figure S11), confirming the zero-charge state of the cluster, consistent with the SCXRD and ESI-MS data.

TD-DFT provides further insight into the nature of the prominent excitations at ~440 and ~560 nm. The strongest contributions to these excitations come from transitions from the HOMO to the LUMO+9 and LUMO+10 and to the LUMO+2, respectively. All of these orbitals are centered on the Ag atoms, with negligible contribution from the Pt atoms (Figure 4). Other optical transitions and the responsible molecular orbitals are given in Table S2 and Figure S12.

Furthermore, the cluster shows a photoluminescence peak at 678 nm (quantum yield ≈ 0.2) upon optical excitation at 442 nm (Figure S13). Nanosecond pump−probe analysis[29] showed a good match of the decay lifetime of the ground-state bleach recovery at 490 nm with the excited-state absorption decay at 590 nm (Figure S14), suggesting the formation of a single transient species following the laser pulse excitation. The kinetic analysis of the transient decay yielded a lifetime of 393 ± 23 ns, providing an indication of the long-lived excited state of the predominant ligand-to-metal charge transfer-type transitions similar to those of other doped Ag NCs.[29]

The Pt doping of the cluster was calculated to have a noticeable effect on its optical spectrum. Figure S15 displays the calculated optical spectrum of a hypothetical

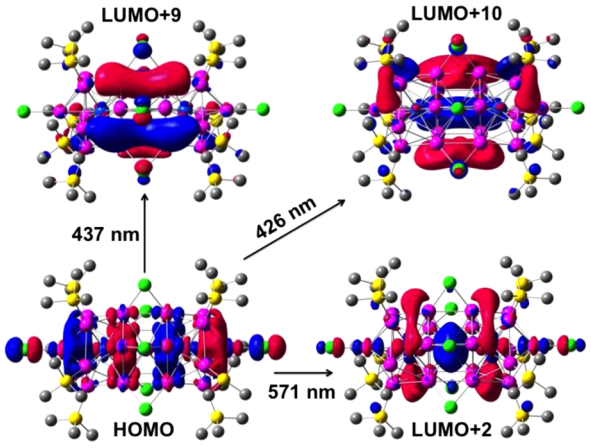

Figure 4. Orbitals with the highest contributions to the transitions at ~440 and ~560 nm. Some atoms have been omitted for clarity.

$[Ag_{25}Cl_7(PPh_3)_{10}]^{2+}$ cluster with 16 free valence s electrons as in $[Pt_2Ag_{23}Cl_7(PPh_3)_{10}]$. Although the shapes of the spectra of the doped and pure Ag clusters are similar, the peaks in the former are blue-shifted by 0.1−0.2 eV. This is due to modulations in the electronic structure caused by heteroatom doping similar to those in other doped Ag NCs.[29,30,40] Notably, the neutral $[Ag_{25}Cl_7(PPh_3)_{10}]$ cluster has a HOMO−LUMO gap of <0.3 eV and a qualitatively different spectrum. The overall effect of Pt dopants on the stability of $[Pt_2Ag_{23}Cl_7(PPh_3)_{10}]$ is revealed by the strongly exothermic DFT mixing energy of Pt and Ag in the cluster (−4.20 eV per two Pt atoms; see the SI for details). Such exothermicity may explain our successful synthesis of the doped clusters but not pure Ag clusters with the same structure.

DFT calculations could attribute the absence of clusters with different degrees of Pt doping to two effects. First, Pt atoms are highly stable at the centers of the two Ag icosahedra compared with other sites on the cluster (Figure S16), and the former sites can accommodate only two Pt atoms (Table S3). Second, $[Pt_2Ag_{23}Cl_7(PPh_3)_{10}]$ clusters appear to be semimagic, i.e., they are 1.35 eV lower in energy than the combination of hypothetical clusters with one and three Pt dopants (see the SI for details). The semimagic nature of $[Pt_2Ag_{23}Cl_7(PPh_3)_{10}]$ can be explained by its semimagic number of 16 valence s electrons.[41] Furthermore, anisotropic NCs such as $[Pt_2Ag_{23}Cl_7(PPh_3)_{10}]$ attain stability from both geometric and electronic factors,[42] unlike spherical NCs,[14,16,23] whose stabilities are explained on the basis of a closed-shell electronic configuration.

In summary, we have successfully synthesized a novel rod-shaped diplatinum-doped silver nanocluster, $[Pt_2Ag_{23}Cl_7(PPh_3)_{10}]$, through the doping strategy. Its crystal structure shows two Pt-centered Ag icosahedra self-assembled by vertex sharing. The chloride ligands were found to protect the cluster through bridging and terminal binding modes. Electronic structure calculations rationalized the effect of Pt dopants on the stability of the cluster, the selective formation of clusters with two Pt atoms, and the origin of the transitions observed in the optical spectra. Our doping approach will motivate researchers to explore different heteroatom-doped Ag nanoclusters to tailor the number of building blocks in the self-assembly, surface structure, and associated properties.

DOI: 10.1021/jacs.6b11875
J. Am. Chem. Soc. 2017, 139, 1053−1056

■ ASSOCIATED CONTENT

Supporting Information

The Supporting Information is available free of charge on the ACS Publications website at DOI: 10.1021/jacs.6b11875.

Synthesis, characterization, and computational details of the $[Pt_2Ag_{23}Cl_7(PPh_3)_{10}]$ cluster (PDF)

Crystallographic data for the $[Pt_2Ag_{23}Cl_7(PPh_3)_{10}]$ cluster (CIF)

■ AUTHOR INFORMATION

Corresponding Authors

*jeanmarie.basset@kaust.edu.sa
*luigi.cavallo@kaust.edu.sa
*osman.bakr@kaust.edu.sa

ORCID

Moussab Harb: 0000-0001-5540-9792
Omar F. Mohammed: 0000-0001-8500-1130
Osman M. Bakr: 0000-0002-3428-1002
Luigi Cavallo: 0000-0002-1398-338X
Jean-Marie Basset: 0000-0003-3166-8882

Notes

The authors declare no competing financial interest.

■ ACKNOWLEDGMENTS

Funding for this work was provided by KAUST. The authors appreciate the Shaheen II supercomputer to support the simulations.

■ REFERENCES

(1) Daniel, M. C.; Astruc, D. *Chem. Rev.* **2004**, *104*, 293.
(2) Jin, R.; Zeng, C.; Zhou, M.; Chen, Y. *Chem. Rev.* **2016**, *116*, 10346.
(3) Zheng, K.; Yuan, X.; Goswami, N.; Zhang, Q.; Xie, J. *RSC Adv.* **2014**, *4*, 60581.
(4) Joshi, C. P.; Bootharaju, M. S.; Bakr, O. M. *J. Phys. Chem. Lett.* **2015**, *6*, 3023.
(5) Mathew, A.; Pradeep, T. *Part. Part. Syst. Charact.* **2014**, *31*, 1017.
(6) Kurashige, W.; Niihori, Y.; Sharma, S.; Negishi, Y. *J. Phys. Chem. Lett.* **2014**, *5*, 4134.
(7) Shichibu, Y.; Negishi, Y.; Watanabe, T.; Chaki, N. K.; Kawaguchi, H.; Tsukuda, T. *J. Phys. Chem. C* **2007**, *111*, 7845.
(8) Wickramasinghe, S.; Atnagulov, A.; Yoon, B.; Barnett, R. N.; Griffith, W. P.; Landman, U.; Bigioni, T. P. *J. Am. Chem. Soc.* **2015**, *137*, 11550.
(9) Bootharaju, M. S.; Dey, R.; Gevers, L. E.; Hedhili, M. N.; Basset, J. M.; Bakr, O. M. *J. Am. Chem. Soc.* **2016**, *138*, 13770.
(10) Salorinne, K.; Malola, S.; Wong, O. A.; Rithner, C. D.; Chen, X.; Ackerson, C. J.; Hakkinen, H. *Nat. Commun.* **2016**, *7*, 10401.
(11) Petty, J. T.; Sergev, O. O.; Ganguly, M.; Rankine, I. J.; Chevrier, D. M.; Zhang, P. *J. Am. Chem. Soc.* **2016**, *138*, 3469.
(12) Femoni, C.; Kaswalder, F.; Iapalucci, M. C.; Longoni, G.; Mehlstaubl, M.; Zacchini, S. *Chem. Commun.* **2005**, 5769.
(13) Biltek, S. R.; Sen, A.; Pedicini, A. F.; Reber, A. C.; Khanna, S. N. *J. Phys. Chem. A* **2014**, *118*, 8314.
(14) Joshi, C. P.; Bootharaju, M. S.; Alhilaly, M. J.; Bakr, O. M. *J. Am. Chem. Soc.* **2015**, *137*, 11578.
(15) Weerawardene, K. L. D. M.; Aikens, C. M. *J. Am. Chem. Soc.* **2016**, *138*, 11202.
(16) AbdulHalim, L. G.; Bootharaju, M. S.; Tang, Q.; Del Gobbo, S.; AbdulHalim, R. G.; Eddaoudi, M.; Jiang, D.-e.; Bakr, O. M. *J. Am. Chem. Soc.* **2015**, *137*, 11970.
(17) Goswami, N.; Yao, Q.; Luo, Z.; Li, J.; Chen, T.; Xie, J. *J. Phys. Chem. Lett.* **2016**, *7*, 962.
(18) Krishnadas, K. R.; Ghosh, A.; Baksi, A.; Chakraborty, I.; Natarajan, G.; Pradeep, T. *J. Am. Chem. Soc.* **2016**, *138*, 140.
(19) Wang, S.; Jin, S.; Yang, S.; Chen, S.; Song, Y.; Zhang, J.; Zhu, M. *Sci. Adv.* **2015**, *1*, e1500441.
(20) Ouyang, R.; Jiang, D.-e. *ACS Catal.* **2015**, *5*, 6624.
(21) Dass, A.; Theivendran, S.; Nimmala, P. R.; Kumara, C.; Jupally, V. R.; Fortunelli, A.; Sementa, L.; Barcaro, G.; Zuo, X.; Noll, B. C. *J. Am. Chem. Soc.* **2015**, *137*, 4610.
(22) Dhayal, R. S.; Liao, J.-H.; Liu, Y.-C.; Chiang, M.-H.; Kahlal, S.; Saillard, J.-Y.; Liu, C. W. *Angew. Chem., Int. Ed.* **2015**, *54*, 3702.
(23) Desireddy, A.; Conn, B. E.; Guo, J.; Yoon, B.; Barnett, R. N.; Monahan, B. M.; Kirschbaum, K.; Griffith, W. P.; Whetten, R. L.; Landman, U.; Bigioni, T. P. *Nature* **2013**, *501*, 399.
(24) Yang, H.; Wang, Y.; Huang, H.; Gell, L.; Lehtovaara, L.; Malola, S.; Häkkinen, H.; Zheng, N. *Nat. Commun.* **2013**, *4*, 2422.
(25) Alhilaly, M. J.; Bootharaju, M. S.; Joshi, C. P.; Besong, T. M.; Emwas, A.-H.; Juarez-Mosqueda, R.; Kaappa, S.; Malola, S.; Adil, K.; Shkurenko, A.; Häkkinen, H.; Eddaoudi, M.; Bakr, O. M. *J. Am. Chem. Soc.* **2016**, *138*, 14727.
(26) Yang, H.; Wang, Y.; Chen, X.; Zhao, X.; Gu, L.; Huang, H.; Yan, J.; Xu, C.; Li, G.; Wu, J.; Edwards, A. J.; Dittrich, B.; Tang, Z.; Wang, D.; Lehtovaara, L.; Häkkinen, H.; Zheng, N. *Nat. Commun.* **2016**, *7*, 12809.
(27) Tofanelli, M. A.; Ni, T. W.; Phillips, B. D.; Ackerson, C. J. *Inorg. Chem.* **2016**, *55*, 999.
(28) Yan, N.; Liao, L.; Yuan, J.; Lin, Y.-j.; Weng, L.-h.; Yang, J.; Wu, Z. *Chem. Mater.* **2016**, *28*, 8240.
(29) Bootharaju, M. S.; Joshi, C. P.; Parida, M. R.; Mohammed, O. F.; Bakr, O. M. *Angew. Chem.* **2016**, *128*, 934.
(30) Soldan, G.; Aljuhani, M. A.; Bootharaju, M. S.; AbdulHalim, L. G.; Parida, M. R.; Emwas, A.-H.; Mohammed, O. F.; Bakr, O. M. *Angew. Chem.* **2016**, *128*, 5843.
(31) Bootharaju, M. S.; Sinatra, L.; Bakr, O. M. *Nanoscale* **2016**, *8*, 17333.
(32) Jin, R.; Liu, C.; Zhao, S.; Das, A.; Xing, H.; Gayathri, C.; Xing, Y.; Rosi, N. L.; Gil, R. R.; Jin, R. *ACS Nano* **2015**, *9*, 8530.
(33) Wang, S.; Meng, X.; Das, A.; Li, T.; Song, Y.; Cao, T.; Zhu, X.; Zhu, M.; Jin, R. *Angew. Chem., Int. Ed.* **2014**, *53*, 2376.
(34) Teo, B. K.; Keating, K. *J. Am. Chem. Soc.* **1984**, *106*, 2224.
(35) Teo, B. K.; Zhang, H.; Shi, X. *Inorg. Chem.* **1994**, *33*, 4086.
(36) Kappen, T. G. M. M.; Schlebos, P. P. J.; Bour, J. J.; Bosman, W. P.; Smits, J. M. M.; Beurskens, P. T.; Steggerda, J. J. *Inorg. Chem.* **1994**, *33*, 754.
(37) Teo, B. K.; Shi, X.; Zhang, H. *J. Am. Chem. Soc.* **1991**, *113*, 4329.
(38) Kang, X.; Xiong, L.; Wang, S.; Yu, H.; Jin, S.; Song, Y.; Chen, T.; Zheng, L.; Pan, C.; Pei, Y.; Zhu, M. *Chem. - Eur. J.* **2016**, *22*, 17145.
(39) Teo, B. K.; Zhang, H.; Shi, X. *J. Am. Chem. Soc.* **1990**, *112*, 8552.
(40) Yan, J.; Su, H.; Yang, H.; Malola, S.; Lin, S.; Häkkinen, H.; Zheng, N. *J. Am. Chem. Soc.* **2015**, *137*, 11880.
(41) Knoppe, S.; Lehtovaara, L.; Häkkinen, H. *J. Phys. Chem. A* **2014**, *118*, 4214.
(42) Wan, X. K.; Yuan, S. F.; Lin, Z. W.; Wang, Q. M. *Angew. Chem., Int. Ed.* **2014**, *53*, 2923.

DOI: 10.1021/jacs.6b11875
J. Am. Chem. Soc. 2017, 139, 1053−1056